JGR Solid Earth

RESEARCH ARTICLE
10.1029/2023JB027556

Crustal and Uppermost Mantle Azimuthal Seismic Anisotropy of Antarctica From Ambient Noise Tomography

Zhengyang Zhou[1,2], Douglas A. Wiens[1], Andrew A. Nyblade[3], Richard C. Aster[4], Terry Wilson[5], and Weisen Shen[6]

[1]Department of Earth and Planetary Sciences, Washington University in St Louis, St Louis, MO, USA, [2]Now at Department of Earth Sciences, University of Minnesota—Twin Cities, Minneapolis, MN, USA, [3]Department of Geosciences, Penn State University, State College, PA, USA, [4]Department of Geosciences and Warner College of Natural Resources, Colorado State University, Fort Collins, CO, USA, [5]School of Earth Sciences, Ohio State University, Columbus, OH, USA, [6]Department of Geosciences, Stony Brook University, Stony Brook, NY, USA

Abstract Seismic anisotropy provides essential information for characterizing the orientation of deformation and flow in the crust and mantle. The isotropic structure of the Antarctic crust and upper mantle has been determined by previous studies, but the azimuthal anisotropy structure has only been constrained by mantle core phase (SKS) splitting observations. This study determines the azimuthal anisotropic structure of the crust and mantle beneath the central and West Antarctica based on 8—55 s Rayleigh wave phase velocities from ambient noise cross-correlation. An anisotropic Rayleigh wave phase velocity map was created using a ray—based tomography method. These data are inverted using a Bayesian Monte Carlo method to obtain an azimuthal anisotropy model with uncertainties. The azimuthal anisotropy structure in most of the study region can be fit by a two-layer structure, with one layer at depths of 0–15 km in the shallow crust and the other layer in the uppermost mantle. The azimuthal anisotropic layer in the shallow crust of West Antarctica, where it coincides with strong positive radial anisotropy quantified by the previous study, shows a fast direction that is subparallel to the inferred extension direction of the West Antarctic Rift System. Fast directions of upper mantle azimuthal anisotropy generally align with teleseismic shear wave splitting fast directions, suggesting a thin lithosphere or similar lithosphere-asthenosphere deformation. However, inconsistencies in this exist in Marie Byrd Land, indicating differing ancient deformation patterns in the shallow mantle lithosphere sampled by the surface waves and deformation in the deeper mantle and asthenosphere sampled more strongly by splitting measurements.

Plain Language Summary Seismic anisotropy, which refers to the directional dependence of seismic wave propagation, provides crucial information about the orientation of deformation and flow within the interior of Earth. While most previous studies have focused on the isotropic structure, our study determines the azimuthal anisotropy structure beneath central and west Antarctica. We found that a two-layer anisotropic structure fits the study region. In West Antarctica, the fast direction of the azimuthal anisotropy in the crust aligns with the extension direction of the West Antarctic Rift System. The agreement between our results and teleseismic core phase studies in the uppermost mantle suggests a thin lithosphere or similar lithosphere-asthenosphere deformation. However, inconsistencies in certain areas of the study region, such as Marie Byrd Land, suggest that the deformation patterns differ between the shallow mantle lithosphere and the deeper mantle asthenosphere. These findings offer new insights into Antarctica's geological history.

Key Points:

- Rayleigh wave phase velocities in Antarctica determined from ambient noise tomography have significant azimuthal anisotropy
- Anisotropy in the upper crust shows fast velocities that are subparallel to the inferred West Antarctic Rift System extension direction
- Mantle fast velocities are often subparallel to core phase splitting directions, suggesting similar lithosphere-asthenosphere anisotropy

Supporting Information:

Supporting Information may be found in the online version of this article.

Correspondence to:

Z. Zhou,
zhou.z@wustl.edu

Citation:

Zhou, Z., Wiens, D. A., Nyblade, A. A., Aster, R. C., Wilson, T., & Shen, W. (2024). Crustal and uppermost mantle azimuthal seismic anisotropy of Antarctica from ambient noise tomography. *Journal of Geophysical Research: Solid Earth*, *129*, e2023JB027556. https://doi.org/10.1029/2023JB027556

Received 26 JUL 2023
Accepted 24 DEC 2023

Author Contributions:

Conceptualization: Zhengyang Zhou, Douglas A. Wiens
Data curation: Douglas A. Wiens, Andrew A. Nyblade, Richard C. Aster, Terry Wilson
Formal analysis: Zhengyang Zhou, Douglas A. Wiens
Funding acquisition: Douglas A. Wiens
Investigation: Zhengyang Zhou
Methodology: Zhengyang Zhou, Weisen Shen

1. Introduction

Unlike other continents, in particular well-instrumented North America and Europe, where seismic anisotropy is relatively well studied (Ai et al., 2020; Lin et al., 2011; Nathan et al., 2021; Zhu et al., 2015, 2017), the seismic anisotropy within the crust and upper mantle of the Antarctic continent is poorly constrained. In the past, there were few detailed studies of the seismic structure of Antarctica, resulting from the lack of instrumentation due to logistical and technical challenges. However, more than 200 broadband seismic stations have been deployed across the Antarctic plate over the last two decades, allowing for a new era of seismic studies of the crust and mantle beneath Antarctica using modern data and methods, including an increasingly detailed understanding of the velocity structure (Hansen et al., 2016; Lloyd et al., 2013, 2020; Shen, Wiens, Stern, et al., 2018; Watson et al., 2006; White-Gaynor et al., 2019; Wiens et al., 2021).

Project Administration: Douglas A. Wiens, Terry Wilson
Resources: Douglas A. Wiens
Software: Zhengyang Zhou, Weisen Shen
Supervision: Douglas A. Wiens
Validation: Zhengyang Zhou, Douglas A. Wiens, Richard C. Aster
Writing – original draft: Zhengyang Zhou
Writing – review & editing: Douglas A. Wiens, Andrew A. Nyblade, Richard C. Aster, Weisen Shen

There have been only sparse prior studies of the anisotropic structure of Antarctica. Several of these have investigated radial (transversely isotropic) anisotropic structure using Rayleigh and Love waves (Cheng et al., 2021; O'Donnell et al., 2019; Zhou et al., 2022). Radial anisotropy measures the difference between horizontal and vertical seismic velocities. Conversely, azimuthal anisotropy describes the variation of seismic velocity with different horizontal propagation direction. Until now, studies of azimuthal seismic anisotropy in Antarctica have employed core (e.g., SKS) shear wave splitting measurements (Accardo et al., 2014; Barklage et al., 2009; Lucas et al., 2022; Reading & Heintz, 2008), which provide detailed measurements of the azimuthal anisotropy beneath individual seismic stations, but lack constraint on the depth distribution of anisotropy.

Shear wave splitting studies that incorporate recently retrieved data indicate a relatively consistent fast polarization direction across much of west Antarctica (Accardo et al., 2014; Lucas et al., 2022) that is generally subparallel to the direction of past extension of the West Antarctica Rift System (WARS). SKS splitting is generally assumed to result from azimuthal anisotropy in the mantle, since the path length in the crust is much smaller than the mantle, and unrealistically large anisotropy would be required to explain some splitting times with crustal anisotropy. Although Global Navigation Satellite Systems (GNSS) and seismicity studies show that the WARS is currently inactive (Donnellan & Luyendyk, 2004; Lucas et al., 2021; Winberry & Anandakrishnan, 2003), deformation fabrics from past tectonic activity can still control the anisotropy characteristics (Lucas et al., 2021). This observation agrees with the assumption that the deformation of olivine, the primary mineral in the mantle, records the lithospheric and sub-lithospheric mantle flow (e.g., Fouch & Rondenay, 2006). Second-order variations in azimuthal anisotropy directions have been observed in other regions of Antarctica, such as Marie Byrd Land (MBL), East Antarctica, and the Whitmore-Ellsworth Mountain region. In these cases, regional tectonic processes and deformation history have been introduced to explain the observations.

A recently developed 3-D transverse isotropic (TI) structure model of Antarctica (Zhou et al., 2022) shows large variations in crustal and uppermost mantle radial anisotropy. A large area in the WARS is dominated by positive anisotropy ($V_{SH} > V_{SV}$) in both the crust and mantle, due to widespread lithosphere-scale extension. Negative anisotropy is found at some depths in the middle and lower crust. The uppermost mantle is characterized by positive anisotropy, with the strongest anisotropy occurring beneath the Transantarctic (TAM) and the Whitmore Mountains. However, the radial anisotropy results provide only a limited picture of the anisotropy variations since they do not characterize azimuthal anisotropic structure.

Rayleigh wave phase velocities can potentially be used to determine azimuthal anisotropy and also provide with additional constraints on the depth distribution of anisotropy, and are thus complementary to SKS splitting studies that reflect the integrated effect of anisotropy along the entire mantle raypath. Global studies have investigated azimuthal anisotropy of the Antarctic region from Rayleigh waves (e.g., Debayle et al., 2016; Schaeffer et al., 2016), but these inversions have large smoothing lengths of many hundreds to thousands of km and thus lack detailed resolution.

In this paper, we analyze Antarctic Rayleigh wave (V_{SV}) azimuthal anisotropy using phase velocities determined from ambient noise crosscorrelation (CC) between data at distinct seismic stations using a two-layer azimuthal anisotropic structure for the study region. By combining the new azimuthally anisotropic structure with the radially anisotropic model of Zhou et al. (2022) a more complete understanding of the seismic anisotropy of the crust and uppermost mantle can be analyzed and discussed. We then discuss and interpret the relationship of the new azimuthal anisotropy results in terms of the previous radial anisotropy and SKS splitting measurements.

2. Data and Method

2.1. Seismic Data in Antarctica

We use the Rayleigh wave phase velocity dispersion measurements between 8 and 55 s obtained by Zhou et al. (2022). Those measurements are obtained from the CC of ambient noise data extracted from 245 broadband seismic stations deployed on the Antarctic continent and surrounding islands, including seven permanent stations (e.g., Ringler et al., 2022) and six large temporary networks (Figure 1, Table S1 in Supporting Information S1). We applied an ambient noise data processing procedure (Bensen et al., 2007) to the data set to extract the surface wave signal between each station pair. We will briefly describe it here. The vertical continuous seismic records were divided into 1-day-long time series, after which we computed the vertical-to-vertical CC followed by time and frequency domain normalization. Then the time-frequency phase weighted stacking (Schimmel &

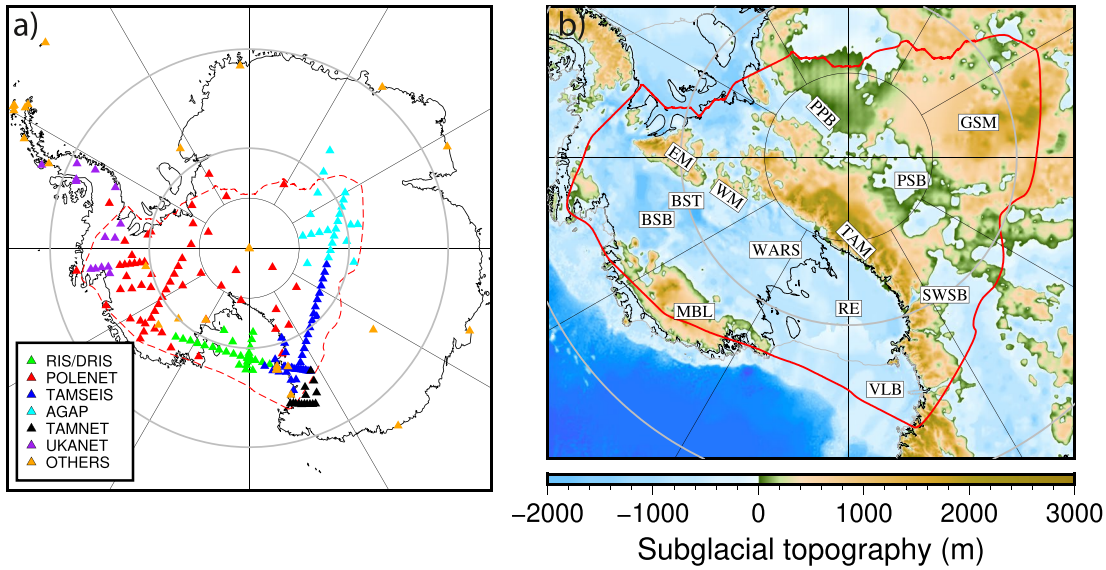

Figure 1. (a) The seismic stations used in this study, with different colors indicating different major networks. The red dotted line outlines the inversion study region. (b) Subglacial topography of the study region with major geological features labeled, again with a red contour enclosing the study region. Abbreviations: GSM—Gamburtsev Subglacial Mountains, PSB—Polar Subglacial Basin, TAM—Transantarctic Mountains, RE—Ross Embayment, MBL—Marie Byrd Land, EM—Ellsworth Mountains. WM—Whitmore Mountains, VLB—Victory Land Basin, SWSB—South Wilkes Subglacial Basin, PPB—Pensacola-Pole Basin, BST—Bentley Subglacial Basin, WARS—West Antarctic Rift System, and BSB—Byrd Subglacial Basin.

Gallart, 2007) was applied to the monthly linear stacked CC to construct the final CC. This non-linear stacking method allows us to expand the period band from 8–40 s to 8–55 s, which is critical to resolving the structure of the deeper uppermost mantle.

2.2. Phase Velocity Azimuthal Anisotropy Tomography

We use a two step inversion method, in which we first determine the Rayleigh wave phase velocities and anisotropy, and then invert them for the depth dependence of anisotropy at each geographical location. In a weakly anisotropic medium, the azimuthal anisotropy of surface wave phase velocity can be represented (Smith & Dahlen, 1973) by

$$C(T,\theta) = C_0(T)\{1 + A_2(T)\cos(2(\theta - \theta_{FA2})) + A_4(T)\cos(4(\theta - \theta_{FA4}))\} \quad (1)$$

where T is the period, θ is the azimuth direction, measured clockwise from the north, $C_0(T)$ is the isotropic phase velocity, $A_2(T)$ and $A_4(T)$ are anisotropic amplitude of the 2θ and 4θ dependence, θ_{FA2} is the 2θ fast-axis direction and θ_{FA4} is the 4θ fast-axis direction. According to previous studies (Feng et al., 2020; Smith & Dahlen, 1973; Xie et al., 2015), the 2θ term typically dominates the azimuthal anisotropy of Rayleigh waves. Given the limited path coverage of the study region and higher azimuthal coverage requirements needed to resolve 4θ dependence, we only solve for the 2θ term of Rayleigh wave phase velocity in this study.

We estimate isotropic phase velocity as well as its azimuthal anisotropy direction and amplitude using a ray-based tomography method with Gaussian regularization (Barmin et al., 2001). To improve the azimuthal coverage and reduce uncertainty, different grid sizes are used for isotropic and azimuthally anisotropic tomography. A set of checkerboard resolution tests with different grid sizes employing synthetic data mimicking actual path coverage was performed to determine optimal grid sizes and test the recovery of anisotropic structure for real data. We found that the tomographic inversion based on a 0.5° by 0.5° grid for isotropic structure with a grid size of 2° by 2° for azimuthal anisotropy shows the best recovery result for simultaneously determining isotropic and azimuthally anisotropic structure. Figure 2 shows the checkerboard test result using final grid settings. The 10-s and 40-s period maps show good recovery in both isotropic and azimuthal anisotropic structures. For the 50-s map, the isotropic structure is still recovered well in the study region, and the azimuthal anisotropy is recovered for the majority of West Antarctica and part of East Antarctica.

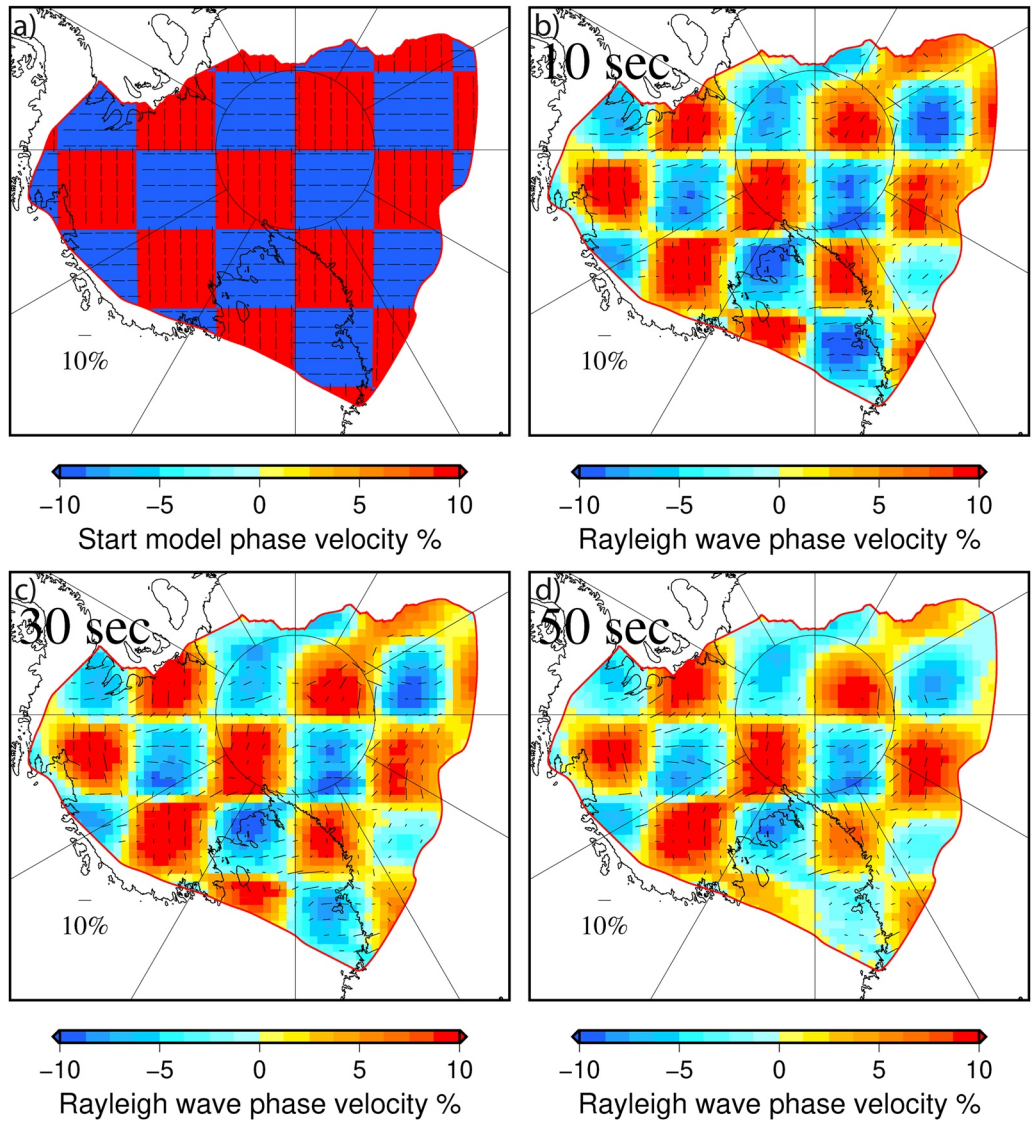

Figure 2. (a) Starting model for checkboard resolution tests utilizing actual data raypaths. Colors denote variation in isotropic phase velocity as denoted in accompanying color bars. The size of each checker is about 500 km by 500 km. The red boundary denotes the isotropic study region. (b–d) Isotropic phase velocity, azimuthal fast axis direction, and amplitude recovery from the actual data path coverage at 10, 30 and 50 s periods.

Quality controls based on path coverage and azimuthal coverage were imposed on the phase velocity and anisotropy maps resulting from the data analysis to ensure that all measurements are reliable. (a)We removed all grid points with less than 100° of azimuthal coverage or 50 total paths to determine the region of well resolved isotropic velocity, denoted by the red boundary on Figures 2 and 3. (b) Within the well resolved isotropic region, we further removed the grid points with less than 180° azimuthal coverage, to define the well resolved region for azimuthal anisotropy. The final maps are constructed from more than 8,000 raypaths, with good results obtained between 8 and 55 s period The region of well resolved azimuthal anisotropy varies by period, with the best results obtained for periods of 15–30 s.

Isotropic phase velocity maps (Figure 3) display strong commonalities with those obtained by previous ambient noise studies (Shen, Wiens, Anandakrishnan, et al., 2018; Zhou et al., 2022). At 10 s period, anisotropy patterns are mainly controlled by the crustal structure and we observe strong anisotropy amplitudes in the RE and GSM regions. At 24 s, isotropic structure shows the characteristic thin crust beneath West Antarctica and much thicker crust beneath East Antarctica (e.g., Chaput et al., 2014; Dunham et al., 2020; Ritzwoller et al., 2001; Shen, Wiens, Stern, et al., 2018). Anisotropic patterns in West Antarctica are sensitive to both the lower crust and uppermost

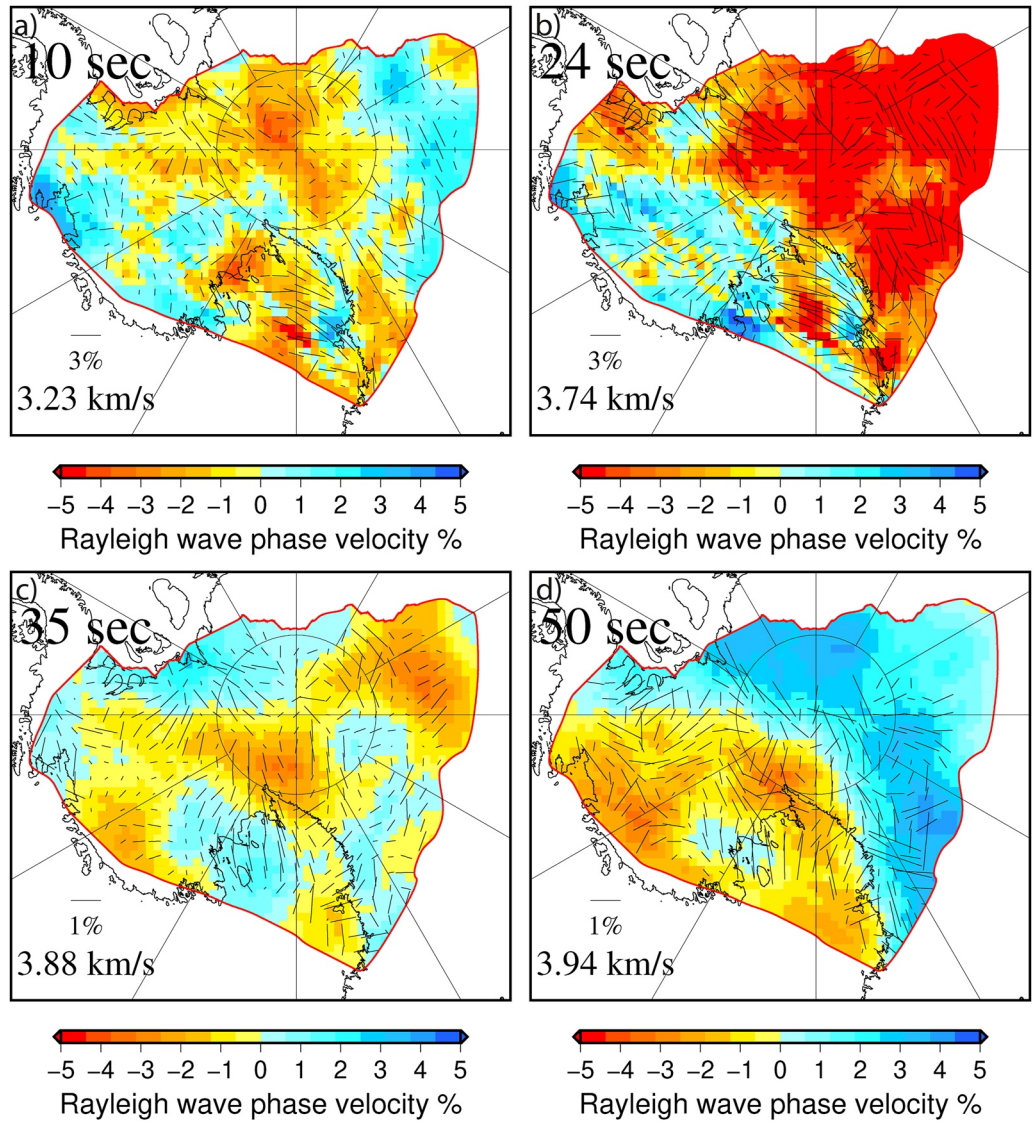

Figure 3. Maps of Rayleigh wave anisotropic phase velocities at 10, 24, 35, and 50 s, respectively. Colors indicates the isotropic velocity variation relative to the average velocity at each reference period shown in the lower left corner. The direction of the small bars show local fast azimuthal directions with length proportional to anisotropic amplitude. The red boundary indicates the study region determined by isotropic velocity-constraining raypath coverage. Bars denoting anisotropic directions are only shown for nodes passing the quality control metrics discussed in the text.

mantle, whereas in East Antarctica the results are still reflecting middle to lower crust anisotropy due to the much thicker crust there. Anisotropy amplitude is generally larger at 24 s than at 10 s. For the 50-s map, the resolvable region in East Antarctica is reduced due to the poorer path coverage, and the results are largely sensitive to upper mantle structure and anisotropy. The absolute amplitude of anisotropy at 35—50 s is noticeably weaker compared with the shorter periods.

We estimate the uncertainty of the isotropic phase velocity from the path density (Shen et al., 2016; Zhou et al., 2022) for each period band. The uncertainties of the azimuthal parameters ($A_2(T)$ and θ_{FA2}) are estimated by error propagation from the isotropic phase velocity uncertainties. The uncertainties are increased by a factor of 1.2 to conservatively account for the weak recovery ability revealed by the checkboard tests.

2.3. Model Parameterization

We use a Bayesian Monte-Carlo method to invert the azimuthally anisotropic Rayleigh wave phase velocity dispersion curves to obtain a 3-D shear wave velocity model including azimuthal anisotropy. The 3-D structure is determined on a grid with 1° spacing by inverting the phase velocities determined for each node to obtain the structure at each depth.

Based on the first-order perturbation theory (Montagner & Nataf, 1986), Rayleigh wave phase velocity (C_R) perturbation can be expressed as

$$\delta C_R(T,\theta) = \int_0^H \begin{bmatrix} \frac{\partial C_R}{\partial A}(\delta A + B_c \cos 2\theta + B_s \sin 2\theta) + \\ \frac{\partial C_R}{\partial F}(\delta F + H_c \cos 2\theta + H_s \sin 2\theta) + \\ \frac{\partial C_R}{\partial L}(\delta L + G_c \cos 2\theta + G_s \sin 2\theta) \end{bmatrix} dz \quad (2)$$

where A, F and L are three of five elastic parameters of the TI medium ($A = \rho V_{\mathrm{PH}}^2$; $C = \rho V_{\mathrm{PV}}^2$; $L = \rho V_{\mathrm{SV}}^2$; $N = \rho V_{\mathrm{SH}}^2$; $F = \eta(A - 2L)$); B_c, B_s, H_c, H_s, G_c and G_s are the amplitude cosine and sine terms of the azimuthal variation; $\frac{\partial C_R}{\partial A}$, $\frac{\partial C_R}{\partial F}$ and $\frac{\partial C_R}{\partial L}$ are the sensitivity kernels of each elastic parameter; H is the maximum depth of the model, and z is the depth.

Rayleigh wave phase velocity is mostly sensitive to the $V_{\mathrm{SV}}(L)$ and $V_{\mathrm{PH}}(A)$ (Feng, 2021; Lin et al., 2011; Yao et al., 2010), so we ignore H_c, H_s terms, which are related to F. We also assume that $\frac{B_{c,s}}{A} = \frac{G_{c,s}}{L}$ as (Lin et al., 2011) Then Equation 2 can be simplified as

$$\delta C_R(T,\theta) = \int_0^H \left[G_c \left(\frac{A}{L}\frac{\partial C_R}{\partial A} + \frac{\partial C_R}{\partial L} \right) \sin 2\theta + G_S \left(\frac{A}{L}\frac{\partial C_R}{\partial A} + \frac{\partial C_R}{\partial L} \right) \cos 2\theta \right] dz \quad (3)$$

The amplitude of the azimuthal anisotropy is $A_{\mathrm{SV}} = \frac{1}{2L}\sqrt{G_c^2 + G_s^2}$ and the fast direction is $\varphi_{\mathrm{SV}} = \frac{1}{2}\arctan\left(\frac{G_S}{G_C}\right)$.

We use the S_{V} component of the 3-D TI structure developed by (Zhou et al., 2022) as the starting model. Depending on the location, the TI structure is constructed by three (sediment, crust, and mantle), four (ice or water, plus 3 solid Earth), or five (ice and water, plus 3 solid Earth) layers and extends to 300 km. For the TI structure, we fix the thickness and seismic velocities of the ice and water (if existing) layer and use the 4 and 6 B-splines functions to describe the shear wave velocity and radial anisotropy in the crust and mantle, respectively. To simplify the azimuthal anisotropic structure, we only allow azimuthal anisotropy in the crust and mantle layer. There is certainly anisotropy in the ice sheet, but the ice layer is too thin and located too near the surface to resolve the ice layer anisotropy.

We tested different crust and mantle azimuthal parameters to determine the most appropriate anisotropy model parameterization. Lack of long period ($T > 55$ s) signal prevents our ambient noise data set from constraining deeper mantle structure, leading to our choice of a single layer for characterizing mantle anisotropy. For choosing the thickness of the mantle anisotropy layer, we performed tests with 80 km thickness through to the entire upper mantle to 300 km. The misfit and results from these thickness parameterization tests show negligible differences, but the 80 km layer thickness model has slightly smaller uncertainty.

Regional crustal structure shows wide thickness velocity structure variation (Shen, Wiens, Anandakrishnan, et al., 2018; Zhou et al., 2022). Crustal thickness varies from about 55 to 18 km, and the much greater thickness in East Antarctica compared to West Antarctica is well resolved. This causes some complexity in choosing a uniform parameterization for anisotropic crustal structure. For the crust, we performed three tests with (a) a single anisotropic layer from the top of the solid Earth to 15 km; (b) a single anisotropic layer encompassing the entire crust; (c) two anisotropic layers, with the first layer from the surface to 15 km depth and the second layer from 15 km to the Moho. Although the 2-layer crustal model allows us to fit the data better for some inversion points and potentially provides a better estimate of the true complexity of the crustal anisotropy, the misfit improvement compared to the 1-layer crustal model is less than 20% for more than two-thirds of the inversion points. Also, for about one-quarter of the inversion points, the azimuthal anisotropy parameters of the lower crustal layer are not constrained by the current data set. For the single layer azimuthal anisotropy through the entire crust (test 2), the misfit is larger than for the single shallow layer (test 1). Based on these tests, we restricted crustal azimuthal

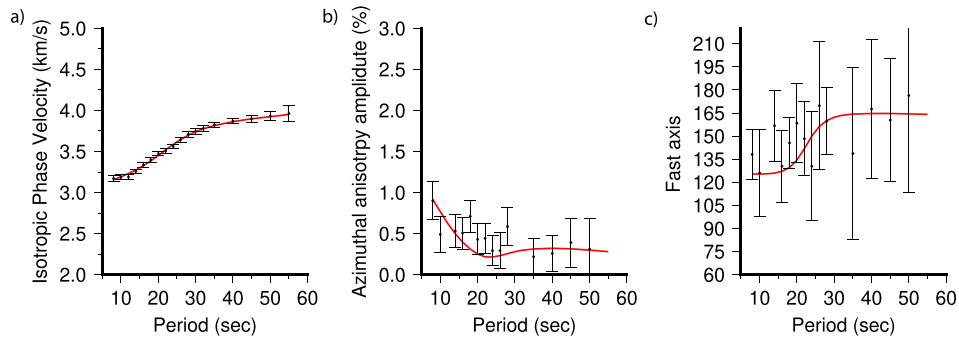

Figure 4. The inversion result for a representative node (86.85°S, 108.33°W). (a) the fit to the isotropic Rayleigh wave phase velocity (red). The black symbols represent observed data, and uncertainty (±1 standard deviation) is shown as the length of the bar (b) and (c) show the amplitude and fast axis of the azimuthal anisotropy; the legends are the same as (a). For this point, the result for crustal azimuthal anisotropy amplitude is 1.4% ± 0.6% with fast axis as 124° ± 12°, and for the mantle is 0.8% ± 0.3% with 167° ± 19°.

anisotropy to the topmost 15 km of the crust. We note that a similar parameterization of the depth distribution of anisotropy has been used in other recent studies of similar data sets, due to the lack of resolution for the anisotropy of the lower crust with ambient noise data (e.g., Feng et al., 2020).

2.4. Bayesian Monte Carlo Inversion

The complete parameterization uses two azimuthal anisotropic structural layers, one in the crust, from the bottom of the sediment to 15 km depth, and one in the uppermost mantle extending down from the Moho, with 80 km thickness. This parameterization does not imply that the lower crust lacks azimuthal anisotropy, but rather results from the inability for the data set to independently resolve azimuthal anisotropy in a lower crustal layer sandwiched between azimuthally anisotropic upper crustal and mantle layers. Since the prior isotropic structure model is well constrained from the Zhou et al. (2022) study using the same Rayleigh wave data set, we limited the perturbation of the V_{SV} structure to 5%. We only invert the Rayleigh wave data set here to introduce azimuthal anisotropy, fixing the V_{SH} structure to that determined by Zhou et al. (2022). For the azimuthal anisotropy, we allowed the amplitude to be perturbed up to 10% with a 180° ambiguity in direction for each azimuthal anisotropy layer. The starting model has zero azimuthal anisotropic amplitude. In summary, there are total of 15 free parameters in the Bayesian Monte Carlo inversion, including 2 in the sedimentary layer (top and bottom velocity), 6 in the crust (2 azimuthal anisotropy parameters in top 15 km, 4 B-spline velocity in the whole crust), 5 in the mantle (2 azimuthal anisotropy parameters in top 80 km, 3 B-spline velocity in the whole mantle) and the thickness of sediment and crust.

One advantage of the Bayesian Monte Carlo inversion method is that uncertainty and trade-off estimates are naturally obtained for parameters from the posterior distribution. As the main goal of this study is to constrain the azimuthal anisotropy, which can be difficult to resolve independent of isotropic shear velocity structure, accurate estimation of uncertainty for the anisotropic parameters is extremely important. Figure 4 shows an example of the inversion results for a representative model node.

3. Results

The results show that the azimuthal anisotropy can be resolved for the two layers throughout most of the study region. Figure 5 shows azimuthal anisotropy results for the crust and mantle plotted on top of the radial anisotropy result modified from (Zhou et al., 2022).

In the majority of the study area, the shallow crust's fast direction aligns with the short-period phase velocity results, while in the mantle, the fast directions is sub-parallel with the result from the longer-period phase velocity map, as anticipated. It is difficult to meaningfully describe fast directions near the South Pole in terms of geographic north, south, east, and west, due to the convergence of latitude lines. Therefore, we use a grid system in the following section, where grid-north is oriented along 0° longitude (upward direction in these maps), grid-south is along 180°, grid-east is along 90°and grid-west is along −90°.

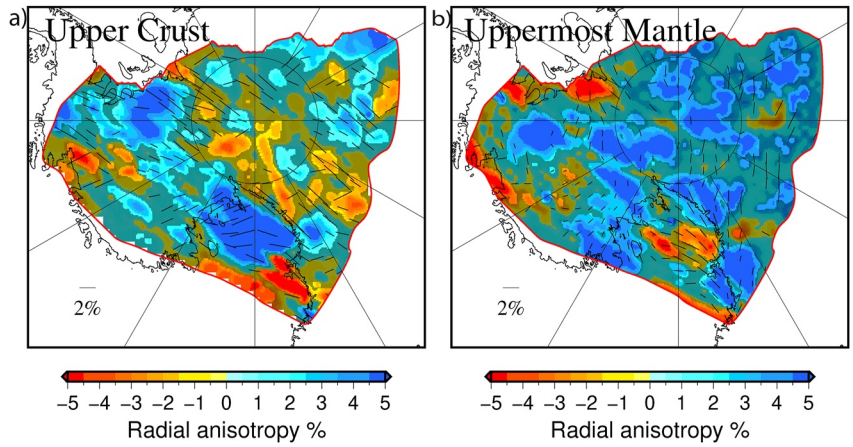

Figure 5. Inversion result of the azimuthal anisotropy for 0–15 km depth in the upper crust (a) and in the uppermost mantle (b) plotted on top of the radial anisotropy from (Zhou et al., 2022) For the crust (a), the radial anisotropy is the average of the upper 15 km of the crust. For the mantle (b), the radial anisotropy is sampled from 15 to 80 km below the Moho depth.

To analyze these azimuthal anisotropy results, we must consider the amplitude and fast direction simultaneously. Large uncertainty in either of them will introduce instability in the other parameter. Therefore, in order to limit the plots to well constrained results, we only show results where (a) the uncertainty of the fast direction is less than 20° and (b) the anisotropy amplitude uncertainty is smaller than half of the actual amplitude.

The average amplitude of the azimuthal anisotropy for the well determined regions of the crust is 2.1%, with an uncertainty of 0.91%. The average uncertainty of the fast direction in the crust is 12.5°. For the crust, regions with strong positive radial anisotropy also show large azimuthal anisotropy amplitude, as observed for the WARS and the Ellsworth-Whitmore Mountains.

For the well resolved region of the mantle, the average amplitude is 1.3% with 0.60% uncertainty, and the average uncertainty of the fast direction is about 16.7°. West Antarctica has a smaller directional uncertainty in the mantle than East Antarctica, due to the better long period coverage and thinner crust, which allows mantle anisotropy to be determined by shorter period Rayleigh waves. Limited by the station coverage and period band, the uppermost mantle azimuthal anisotropy is less well constrained compared with the crustal anisotropy, and the amplitude may be underestimated. However, the average amplitude of this study is similar to that from global-scale multimode Rayleigh wave studies (Debayle et al., 2016; Schaeffer et al., 2016) in the Antarctic region, and the new model provides higher spatial resolution. The average amplitude of this result also agrees with regional studies in other continental regions (e.g., Alaska (Feng et al., 2020), Mediterranean (Feng & Díaz, 2022) and North America *t* (Zhu et al., 2020)).

4. Discussion

4.1. Crustal Anisotropy of the West Antarctic Rift System

A first order feature of the upper crustal result (Figure 5a) is strong azimuthal anisotropy that is correlated with the strong positive radial anisotropy beneath the Southern Ross Embayment and the WARS. It is commonly assumed that shape preferred orientation (SPO) from high-angle cracks and faults, which usually result in negative radial anisotropy, are the dominant source of the shallow crust anisotropy (Feng et al., 2020; Ojo et al., 2017; Xie et al., 2013). Extensional stress during WARS rifting would have opened many faults and cracks; however, GNSS and seismicity studies show that the WARS is currently inactive, and other studies suggest that faults begin healing rapidly after motion ceases (Hiramatsu et al., 2005). In addition, the fast direction of azimuthal anisotropy is subparallel to the to the inferred direction of past extension in the Ross Embayment and the WARS (Siddoway, 2008; Wilson & Luyendyk, 2009), whereas the horizontal fast axis of anisotropy from extensional cracks should be perpendicular to the extension direction. This, combined with the observation of positive radial anisotropy instead of the typical negative radial anisotropy, suggests that the upper crustal anisotropy here cannot be due to extensional cracks.

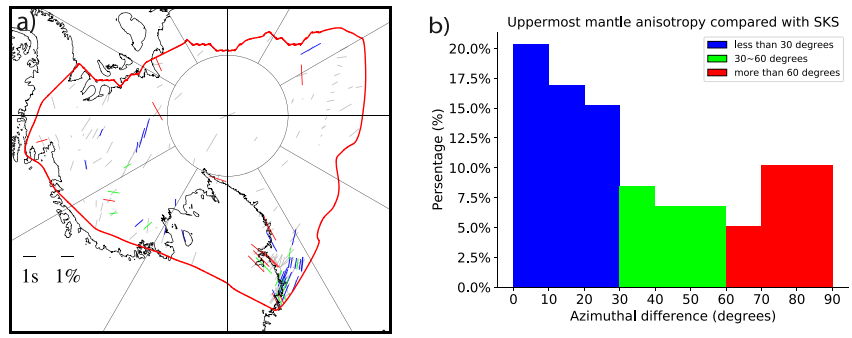

Figure 6. Comparison between fast shear wave direction estimates from station-averaged splitting measurements (Lucas et al., 2022) and uppermost mantle azimuthal anisotropy derived from Rayleigh waves by this study. Data selecton is described in the main text. (a) Map comparing fast axis orientations from shear wave splitting (gray bars) and Rayleigh waves from this study (colored bar ranges show in panel (b)). The different colors represent the different azimuthal differences, with blue indicating differences less 30°, green between 30°—60°, and red 60°—90°. (b) A histogram of the distribution differences in fast axis orientation.

In this case, the association of strong azimuthal anisotropy showing fast axes subparallel to the extension direction with positive radial anisotropy suggests that the anisotropy may result from lattice preferred orientation (LPO). Upper and mid-crustal rocks can show strong LPO due to the orientation of mica and amphibole minerals by deformation (Aster & Shearer, 1992; Dempsey et al., 2011; Ji et al., 2015; Shao et al., 2016). Alignment of these minerals due to deformation introduces directional dependence of bulk seismic velocities shows orthorhombic symmetry. In a region of extension and crustal flow, this may produce strong positive radial anisotropy, with azimuthal anisotropy showing the fast axes pointing in the extension direction. LPO from deformation can persist indefinitely after tectonic activity ceases unless it is overprinted by a later deformational event. With the strong azimuthal anisotropy subparallel with the extension direction and the positive radial anisotropy, we contend that is likely that the shallow crust in the WARS is controlled by the LPO of anisotropic crust minerals instead of SPO from the cracks and faults.

4.2. Mantle Azimuthal Anisotropy

4.2.1. Comparison With Previous Shear Wave Splitting Measurements

It is useful to compare the azimuthal anisotropy results from this study to those of mantle core phase (e.g., SKS) splitting studies (Accardo et al., 2014; Lucas et al., 2022), which constrain azimuthal anisotropy beneath seismic stations and are generally interpreted as measuring upper mantle anisotropy. However, the depth distribution of sensitivity is very different for SKS splitting measurements versus the intermediate-period Rayleigh waves used in this study. SKS splitting measurements are sensitive to azimuthal anisotropy occurring generally anywhere between the core-mantle boundary and the surface, although considerable evidence suggests they typically measure anisotropy in the uppermost 200—300 km of the mantle (Fischer & Wiens, 1996; Savage, 1999). In contrast, this study constrains only a single layer of anisotropy comprising the upper 80 km of the mantle, since the periods with good Rayleigh wave ambient noise results (8–55 s) fail to constrain anisotropy at greater depth. Given that the peak sensitivity of 55 s Rayleigh waves is near 75 km depth (Figure S1 in Supporting Information S1), the results shown here are more sensitive to the anisotropy in the shallowest upper mantle as well as being nonuniformly sensitive to anisotropy throughout the parameterized 80 km thick layer. Therefore the surface wave results characterize anisotropy within a relatively thin layer at the top of the upper mantle, whereas the SKS measurements may reflect an average over several hundred km.

Figure 6 shows a comparison between results from this study and the SKS fast directions from Accardo et al. (2014) and Lucas et al. (2022). To make a reliable comparison, both the SKS measurements and the uppermost mantle azimuthal fast directions are required to satisfy a quality control process and matching procedure based on the distance between the station and the grid point of the azimuthal anisotropy model. First, we only consider station-averaged shear wave splitting measurements with a splitting time greater than 0.5 s, since small splitting times are subject to larger uncertainties and may reflect weak or complicated anisotropy. Second, we associate quality shear wave splitting measurements with the closest node having a high-quality Rayleigh wave anisotropy result, using the quality control outlined in Section 2.1. We require that the distance between the station and the node be less than 60 km to ensure that they sample a similar region of the mantle. We then calculate the angle between the fast directions from

the splitting observation and the Rayleigh wave anisotropy result. Note that the Ross Ice Shelf in the Ross Embayment lacks splitting measurements because the ocean layer beneath the ice shelf precludes the passage of S waves.

We assembled 187 splitting measurements associated with 59 azimuthal anisotropy results (Figure 6). More than 50% of stations indicate less than 30° difference between the fast direction from splitting and from our results for Rayleigh wave azimuthal anisotropy. Most of these are located in the Ross Embayment and the WARS, indicating that in much of West Antarctica the shallow mantle lithosphere sampled by the surface waves and the thicker region including the asthenosphere sampled by the core phase measurements have similar anisotropy patterns. This indicates that the lithosphere and asthenosphere were deformed by similar tectonics and processes in these regions.

In contrast, other regions show larger discrepancies between the quality-controlled fast directions from Rayleigh waves and published shear wave splitting estimates, suggesting that the LPO of the shallow mantle lithosphere is significantly different from the LPO in the asthenosphere in these regions. This is likely due to the lithospheric anisotropy recording deformation from past tectonic episodes, that remains preserved because of the cold temperatures. In contrast, the asthenosphere sampled by the core phases may reflect present-day mantle flow processes.

4.2.2. Mantle Azimuthal Fast Axis Patterns and Interpretation

Our mantle azimuthal anisotropy results show some distinct patterns (Figure 5b). For the TAM (grid east of the Ross Embayment) the observed strong grid NE—SW azimuthal fast direction is consistent with a previous study using teleseismic earthquake Rayleigh waves (Lawrence et al., 2006), as well as shear wave splitting measurements (Barklage et al., 2009; Figure 6). This fast direction is consistant with LPO induced by Cenezoic extension of the Ross Sea region or by mantle flow caused by edge-driven convection associated with the boundary of cold East Antarctic lithosphere (Barklage et al., 2009). Along the Ross Sea coast, our fast direction estimates change to grid NW--SE, and there is a large discrepancy between splitting measurements and surface wave results (Figure 6a). The may result from the larger geographic averaging of the surface wave results relative to the core phase measurements, which are sensitive to only the structure immediately beneath the station. Alternatively, this may reflect differing depth resolution between the two methods; for example, there may be a two-layered anisotropy structure in the mantle, where the surface wave results indicating grid NW–SE fast directions in the lithosphere and the splitting measurements consistent with NS fast directions in the asthenosphere.

In the WARS, to the grid west of the Ross Embayment, the fast azimuthal axis changes to grid NE–SW. A similar direction is found along the boundary between the WARS and the Whitmore Mountains, where previous studies found extremely strong (>1 s) and consistent shear wave splitting patterns (Accardo et al., 2014; Lucas et al., 2022). These fast directions are subparallel with the general extension direction in the WARS, consistent with a mantle olivine LPO oriented by tectonic extensional deformation. The good fit between the surface wave results and the splitting measurements, as well as the generally large splitting times are consistent with a thick layer of uniformly oriented azimuthal anisotropy in the mantle.

For the MBL region, although there are only three stations satisfying the comparison criteria, all intercomparisons show poor fits between splitting measurements and our results. This indicates a difference between the anisotropy in the shallow mantle lithosphere detected by the surface wave result and the deeper signal of mantle flow in the asthenosphere recorded by SKS splitting. Considering evidence suggesting a disrupted mantle plume beneath the MBL dome (Emry et al., 2015; Lloyd et al., 2015; Panter et al., 1997; Sims et al., 2021), a complicated deep mantle anisotropy structure may be expected, and this could explain the differences between the splitting and surface wave results. The anisotropy pattern of the mantle plumes predicted by geodynamic models (Druken et al., 2013) indicates a complex fast direction at different depths, where the deeper portion is perpendicular to the radial flow pattern, and the shallow part is approximately parallel to the radial flow direction, for instance.

This study shows relatively low azimuthal anisotropy amplitudes with larger uncertainties across East Antarctica and results do not pass the quality controls at most locations. Compared with West Antarctica, the thicker crust and limited data coverage at 45–55 s (Figure 3) in East Antarctica constrain our ability to image mantle anisotropy using surface waves. The uppermost mantle in East Antarctica may also have lower anisotropy amplitudes due to its cratonic setting and lack of recent tectonic activity, as suggested by a previous study using teleseismic earthquake Rayleigh waves (Heeszel et al., 2013) and the small magnitude of most shear wave splitting measurements (Lucas et al., 2022) in the region. Studies in other regions also suggest that continental cratonic lithosphere shows smaller mantle azimuthal anisotropy than is found in regions of recent tectonic activity (e.g., Chen et al., 2021).

5. Conclusions

We present a new model of crust and uppermost mantle azimuthal anisotropic structure beneath West and Central Antarctica derived from ambient noise Rayleigh wave observations between 8 and 55 s. Due to the limited frequency content of these data, lower crustal azimuthal anisotropy cannot be constrained by the data set. We parameterize the model using a two-layer azimuthal anisotropic structure, with one layer in the shallow crust down to 15 km depth and the other layer in the uppermost mantle to 80 km. The use of a Bayesian Monte-Carlo inversion allows quantification of uncertainties and anisotropy is only interpreted in regions where this indicates that anisotropic parameters are well resolved.

Combined with recently obtained radial anisotropy results (Zhou et al., 2022), our results reveal (a) strong azimuthal and radial anisotropy in the shallow crust beneath the WARS, which we interpret as being caused by the LPO of crustal minerals during a long history of tectonic extension (b) widespread azimuthal anisotropy with a grid NW–SE fast axis in the WARS (grid west of the Ross Embayment) and near the boundary of the WARS and the Whitmore Mountains. This orientation is subparallel with inferred direction of past extension along the WARS and is consistent with strong shear wave splitting measurements. This is consistent with both the uppermost mantle and the deeper asthenosphere are characterized by deformation patterns resulting from tectonic extension. (c) In the MBL region, there is a discrepancy between the azimuthal anisotropy from Rayleigh waves and shear wave splitting measurements, indicating that the shallowest mantle lithosphere differs anisotropically compared to asthenospheric mantle, and that anisotropy may be perturbed by mantle flow associated with the MBL mantle plume. (d) The mantle anisotropy of East Antarctica is more difficult to characterize due to thicker crust and limitations of data, and results are consistent with lesser intrinsic lower magnitude of uppermost mantle azimuthal anisotropy in this cratonic region.

This study provides the first model of the azimuthal anisotropy of the crust and uppermost mantle beneath West and central Antarctica from regional distance surface waves derived from ambient noise. As more data become available, higher resolution models of anisotropy as well as longer period studies using earthquake data will provide a more complete model of anisotropy, to further advance understanding of the tectonics, deformation, and mantle flow beneath the Antarctic continent.

Data Availability Statement

All raw seismic data used in this study are available without restriction through the Earthscope Data Management Center (https://ds.iris.edu/ds/nodes/dmc/), including station with network identifiers 1D (Brisbourne et al., 2016), YT (Wiens et al., 2007), ZJ (Hansen, 2012), ZM (Wiens & Nyblade, 2007), XP (Anandakrishnan et al., 2000), and XH (Wiens et al., 2014). All figures are made with Generic Mapping Tools version 6 (Wessel et al., 2019), available at https://www.generic-mapping-tools.org/.

Acknowledgments
The authors thank the support of all field teams who collected the data, especially Patrick Shore and Andrew J. Lloyd. This work is supported by the National Science Foundation (NSF) under grants OPP-1744889 (Douglas A. Wiens), OPP-1945693 (Douglas A. Wiens), OPP-1945856 (Weisen Shen) and EAR-1600087 (Weisen Shen). Many of the seismic stations in this study were supported by EarthScope Consortium through the PASSCAL Polar Support Services. The facilities of the Earthscope Data Management Center (https://ds.iris.edu/ds/nodes/dmc/) were used for access data used in this study. Global Seismographic Network is a cooperative scientific facility operated jointly by the NSF and the United States Geological Survey. The NSF component is part of NSF's SAGE Facility, operated by EarthScope Consortium. The facilities of EarthScope Consortium were used for access to waveforms, related metadata, and/or derived products used in this study. These services are funded through the Seismological Facility for the Advancement of Geoscience (SAGE) Award of the NSF under Cooperative Support Agreement EAR-1851048 and OPP-1851037.

References

Accardo, N., Wiens, D., Hernandez, S., Aster, R., Nyblade, A., Huerta, A., et al. (2014). Upper mantle seismic anisotropy beneath the West Antarctic Rift System and surrounding region from shear wave splitting analysis. *Geophysical Journal International*, *198*(1), 414–429. https://doi.org/10.1093/gji/ggu117

Ai, S., Zheng, Y., & Wang, S. (2020). Crustal deformations of the central north China craton constrained by radial anisotropy. *Journal of Geophysical Research: Solid Earth*, *125*(7). https://doi.org/10.1029/2019jb018374

Anandakrishnan, S., Wiens, D., & Nyblade, A. (2000). A broadband seismic investigation of deep continental structure across the east-west Antarctic boundary [Dataset]. International Federation of Digital Seismograph Networks. https://doi.org/10.7914/SN/XP_2000

Aster, R. C., & Shearer, P. M. (1992). Initial shear-wave particle motions and stress constraints at the Anza seismic network. *Geophysical Journal International*, *108*(3), 740–748. https://doi.org/10.1111/j.1365-246X.1992.tb03465.x

Barklage, M., Wiens, D. A., Nyblade, A., & Anandakrishnan, S. (2009). Upper mantle seismic anisotropy of South Victoria Land and the Ross Sea coast, Antarctica from SKS and SKKS splitting analysis. *Geophysical Journal International*, *178*(2), 729–741. https://doi.org/10.1111/j.1365-246x.2009.04158.x

Barmin, M., Ritzwoller, M., & Levshin, A. (2001). A fast and reliable method for surface wave tomography. *Pure and Applied Geophysics*, *158*(8), 1351–1375. https://doi.org/10.1007/pl00001225

Bensen, G. D., Ritzwoller, M. H., Barmin, M. P., Levshin, A. L., Lin, F., Moschetti, M. P., et al. (2007). Processing seismic ambient noise data to obtain reliable broad-band surface wave dispersion measurements. *Geophysical Journal International*, *169*(3), 1239–1260. https://doi.org/10.1111/j.1365-246X.2007.03374.x

Brisbourne, A., Stuart, G., & O'Donnell, J. P. (2016). UKANET: UK Antarctic network [Dataset]. International Federation of Digital Seismograph Networks. https://doi.org/10.7914/SN/1D_2016

Chaput, J., Aster, R., Huerta, A. D., Sun, X., Lloyd, A., Wiens, D., et al. (2014). The crustal thickness of West Antarctica. *Journal of Geophysical Research*, *119*, 1–18. https://doi.org/10.1002/2013JB010642

Chen, X., Levin, V., & Yuan, H. (2021). Small shear wave splitting delays suggest weak anisotropy in cratonic mantle lithosphere. *Geophysical Research Letters*, *48*(16). https://doi.org/10.1029/2021gl093861

Cheng, W., Hu, X. G., & Liu, L. T. (2021). Anisotropy gradients in the middle of the Ross Sea Embayment, west Antarctica: Evidence from QL scattered surface waves. *Geophysical Research Letters*, *48*(6). https://doi.org/10.1029/2020gl091232

Debayle, E., Dubuffet, F., & Durand, S. (2016). An automatically updated S-wave model of the upper mantle and the depth extent of azimuthal anisotropy. *Geophysical Research Letters*, *43*(2), 674–682. https://doi.org/10.1002/2015gl067329

Dempsey, E. D., Prior, D. J., Mariani, E., Toy, V. G., & Tatham, D. J. (2011). Mica-controlled anisotropy within mid-to-upper crustal mylonites: An EBSD study of mica fabrics in the Alpine Fault Zone, New Zealand. *Geological Society, London, Special Publications*, *360*(1), 33–47. https://doi.org/10.1144/sp360.3

Donnellan, A., & Luyendyk, B. P. (2004). GPS evidence for a coherent Antarctic plate and for postglacial rebound in Marie Byrd Land. *Global and Planetary Change*, *42*(1–4), 305–311. https://doi.org/10.1016/j.gloplacha.2004.02.006

Druken, K. A., Kincaid, C., & Griffiths, R. W. (2013). Directions of seismic anisotropy in laboratory models of mantle plumes. *Geophysical Research Letters*, *40*(14), 3544–3549. https://doi.org/10.1002/grl.50671

Dunham, C. K., O'Donnell, J. P., Stuart, G. W., Brisbourne, A. M., Rost, S., Jordan, T. A., et al. (2020). A joint inversion of receiver function and Rayleigh wave phase velocity dispersion data to estimate crustal structure in west Antarctica. *Geophysical Journal International*, *223*(3), 1644–1657. https://doi.org/10.1093/gji/ggaa398

Emry, E. L., Nyblade, A. A., Julià, J., Anandakrishnan, S., Aster, R. C., Wiens, D. A., et al. (2015). The mantle transition zone beneath West Antarctica: Seismic evidence for hydration and thermal upwellings. *Geochemistry, Geophysics, Geosystems*, *16*(1), 40–58. https://doi.org/10.1002/2014gc005588

Feng, L. (2021). Amphibious shear wave structure beneath the Alaska-Aleutian subduction zone from ambient noise tomography. *Geochemistry, Geophysics, Geosystems*, *22*(5). https://doi.org/10.1029/2020gc009438

Feng, L., & Díaz, J. (2022). Azimuthal anisotropy of the westernmost Mediterranean: New constraints on lithospheric deformation and geodynamical evolution. *Earth and Planetary Science Letters*, *593*, 117689. https://doi.org/10.1016/j.epsl.2022.117689

Feng, L., Liu, C., & Ritzwoller, M. H. (2020). Azimuthal anisotropy of the crust and uppermost mantle beneath Alaska. *Journal of Geophysical Research: Solid Earth*, *125*(12). https://doi.org/10.1029/2020jb020076

Fischer, K. M., & Wiens, D. A. (1996). The depth distribution of mantle anisotropy beneath the Tonga subduction zone. *Earth and Planetary Science Letters*, *142*(1–2), 253–260. https://doi.org/10.1016/0012-821x(96)00084-2

Fouch, M. J., & Rondenay, S. (2006). Seismic anisotropy beneath stable continental interiors. *Physics of the Earth and Planetary Interiors*, *158*(2–4), 292–320. https://doi.org/10.1016/j.pepi.2006.03.024

Hansen, S. (2012). Transantarctic Mountains northern network [Dataset]. International Federation of Digital Seismograph Networks. https://doi.org/10.7914/SN/ZJ_2012

Hansen, S. E., Kenyon, L. M., Graw, J. H., Park, Y., & Nyblade, A. A. (2016). Crustal structure beneath the Northern Transantarctic Mountains and Wilkes Subglacial Basin: Implications for tectonic origins. *Journal of Geophysical Research: Solid Earth*, *121*(2), 812–825. https://doi.org/10.1002/2015jb012325

Heeszel, D. S., Wiens, D. A., Nyblade, A. A., Hansen, S. E., Kanao, M., An, M., & Zhao, Y. (2013). Rayleigh wave constraints on the structure and tectonic history of the Gamburtsev Subglacial Mountains, East Antarctica. *Journal of Geophysical Research: Solid Earth*, *118*(5), 2138–2153. https://doi.org/10.1002/jgrb.50171

Hiramatsu, Y., Honma, H., Saiga, A., Furumoto, M., & Ooida, T. (2005). Seismological evidence on characteristic time of crack healing in the shallow crust. *Geophysical Research Letters*, *32*(9). https://doi.org/10.1029/2005gl022657

Ji, S., Shao, T., Michibayashi, K., Oya, S., Satsukawa, T., Wang, Q., et al. (2015). Magnitude and symmetry of seismic anisotropy in mica- and amphibole-bearing metamorphic rocks and implications for tectonic interpretation of seismic data from the southeast Tibetan Plateau. *Journal of Geophysical Research: Solid Earth*, *120*(9), 6404–6430. https://doi.org/10.1002/2015jb012209

Lawrence, J. F., Wiens, D. A., Nyblade, A. A., Anandakrishnan, S., Shore, P. J., & Voigt, D. (2006). Upper mantle thermal variations beneath the Transantarctic Mountains inferred from teleseismic S-wave attenuation. *Geophysical Research Letters*, *33*(3). https://doi.org/10.1029/2005gl024516

Lin, F.-C., Ritzwoller, M. H., Yang, Y., Moschetti, M. P., & Fouch, M. J. (2011). Complex and variable crustal and uppermost mantle seismic anisotropy in the western United States. *Nature Geoscience*, *4*(1), 55–61. https://doi.org/10.1038/ngeo1036

Lloyd, A. J., Nyblade, A. A., Wiens, D. A., Hansen, S. E., Kanao, M., Shore, P. J., & Zhao, D. (2013). Upper mantle seismic structure beneath central East Antarctica from body wave tomography: Implications for the origin of the Gamburtsev Subglacial Mountains. *Geochemistry, Geophysics, Geosystems*, *14*(4), 902–920. https://doi.org/10.1002/ggge.20098

Lloyd, A. J., Wiens, D. A., Nyblade, A. A., Anandakrishnan, S., Aster, R. C., Huerta, A. D., et al. (2015). A seismic transect across West Antarctica: Evidence for mantle thermal anomalies beneath the Bentley Subglacial Trench and the Marie Byrd Land Dome. *Journal of Geophysical Research: Solid Earth*, *120*(12), 8439–8460. https://doi.org/10.1002/2015jb012455

Lloyd, A. J., Wiens, D. A., Zhu, H., Tromp, J., Nyblade, A. A., Aster, R. C., et al. (2020). Seismic structure of the Antarctic upper mantle imaged with adjoint tomography. *Journal of Geophysical Research: Solid Earth*, *125*(3). https://doi.org/10.1029/2019jb017823

Lucas, E. M., Nyblade, A. A., Accardo, N. J., Lloyd, A. J., Wiens, D. A., Aster, R. C., et al. (2022). Shear wave splitting across Antarctica: Implications for upper mantle seismic anisotropy. *Journal of Geophysical Research: Solid Earth*, *127*(4). https://doi.org/10.1029/2021jb023325

Lucas, E. M., Nyblade, A. A., Lloyd, A. J., Aster, R. C., Wiens, D. A., O'Donnell, J. P., et al. (2021). Seismicity and Pn velocity structure of central West Antarctica. *Geochemistry, Geophysics, Geosystems*, *22*(2). https://doi.org/10.1029/2020gc009471

Montagner, J., & Nataf, H. (1986). A simple method for inverting the azimuthal anisotropy of surface waves. *Journal of Geophysical Research*, *91*(B1), 511–520. https://doi.org/10.1029/jb091ib01p00511

Nathan, E. M., Hariharan, A., Florez, D., & Fischer, K. M. (2021). Multi-layer seismic anisotropy beneath Greenland. *Geochemistry, Geophysics, Geosystems*, *22*(5). https://doi.org/10.1029/2020gc009512

O'Donnell, J. P., Brisbourne, A. M., Stuart, G. W., Dunham, C. K., Yang, Y., Nield, G. A., et al. (2019). Mapping crustal shear wave velocity structure and radial anisotropy beneath west Antarctica using seismic ambient noise. *Geochemistry, Geophysics, Geosystems*, *20*(11), 5014–5037. https://doi.org/10.1029/2019gc008459

Ojo, A. O., Ni, S., & Li, Z. (2017). Crustal radial anisotropy beneath Cameroon from ambient noise tomography. *Tectonophysics*, *696–697*, 37–51. https://doi.org/10.1016/j.tecto.2016.12.018

Panter, K. S., Kyle, P. R., & Smellie, J. L. (1997). Petrogenesis of a phonolite–Trachyte succession at Mount Sidley, Marie Byrd Land, Antarctica. *Journal of Petrology*, *38*(9), 1225–1253. https://doi.org/10.1093/petroj/38.9.1225

Reading, A. M., & Heintz, M. (2008). Seismic anisotropy of East Antarctica from shear-wave splitting: Spatially varying contributions from lithospheric structural fabric and mantle flow? *Earth and Planetary Science Letters*, *268*(3–4), 433–443. https://doi.org/10.1016/j.epsl.2008.01.041

Ringler, A. T., Anthony, R. E., Aster, R. C., Ammon, C. J., Arrowsmith, S., Benz, H., et al. (2022). Achievements and prospects of global broadband seismographic networks after 30 Years of continuous geophysical observations. *Reviews of Geophysics*, *60*(3). https://doi.org/10.1029/2021rg000749

Ritzwoller, M. H., Shapiro, N. M., Levshin, A. L., & Leahy, G. M. (2001). Crustal and upper mantle structure beneath Antarctica and surrounding oceans. *Journal of Geophysical Research*, *106*(B12), 30645–30670. https://doi.org/10.1029/2001jb000179

Savage, M. K. (1999). Seismic anisotropy and mantle deformation: What have we learned from shear wave splitting? *Reviews of Geophysics*, *37*(1), 65–106. https://doi.org/10.1029/98rg02075

Schaeffer, A. J., Lebedev, S., & Becker, T. W. (2016). Azimuthal seismic anisotropy in the Earth's upper mantle and the thickness of tectonic plates. *Geophysical Journal International*, *207*(2), 901–933. https://doi.org/10.1093/gji/ggw309

Schimmel, M., & Gallart, J. (2007). Frequency-dependent phase coherence for noise suppression in seismic array data. *Journal of Geophysical Research*, *112*(B4). https://doi.org/10.1029/2006jb004680

Shao, T., Ji, S., Oya, S., Michibayashi, K., & Wang, Q. (2016). Mica-dominated seismic properties of mid-crust beneath west Yunnan (China) and geodynamic implications. *Tectonophysics*, *677*(678), 324–338. https://doi.org/10.1016/j.tecto.2016.04.024

Shen, W., Ritzwoller, M. H., Kang, D., Kim, Y., Lin, F.-C., Ning, J., et al. (2016). A seismic reference model for the crust and uppermost mantle beneath China from surface wave dispersion. *Geophysical Journal International*, *206*(2), 954–979. https://doi.org/10.1093/gji/ggw175

Shen, W., Wiens, D. A., Anandakrishnan, S., Aster, R. C., Gerstoft, P., Bromirski, P. D., et al. (2018). The crust and upper mantle structure of central and West Antarctica from Bayesian inversion of Rayleigh wave and receiver functions. *Journal of Geophysical Research: Solid Earth*, *123*(9), 7824–7849. https://doi.org/10.1029/2017JB015346

Shen, W., Wiens, D. A., Stern, T., Anandakrishnan, S., Aster, R. C., Dalziel, I., et al. (2018). Seismic evidence for lithospheric foundering beneath the southern Transantarctic Mountains, Antarctica. *Geology*, *46*(1), 71–74. https://doi.org/10.1130/G39555.1

Siddoway, C. S. (2008). Tectonics of the West Antarctic Rift System: New light on the history and dynamics of distributed intracontinental extension. In *Antarctica: A keystone in a changing world* (pp. 91–114). https://doi.org/10.3133/ofr20071047kp09

Sims, K. W. W., Aster, R. C., Gaetani, G., Blichert-Toft, J., Phillips, E. H., Wallace, P. J., et al. (2021). Chapter 7.2 Mount Erebus. In *Memoirs*. Geological Society. https://doi.org/10.1144/m55-2019-8

Smith, M. L., & Dahlen, F. A. (1973). The azimuthal dependence of Love and Rayleigh wave propagation in a slightly anisotropic medium. *Journal of Geophysical Research*, *78*(17), 3321–3333. https://doi.org/10.1029/jb078i017p03321

Watson, T., Nyblade, A., Wiens, D. A., Anandakrishnan, S., Benoit, M., Shore, P. J., et al. (2006). P and S velocity structure of the upper mantle beneath the Transantarctic Mountains, East Antarctic craton, and Ross Sea from travel time tomography: Mantle P and S velocity structure. *Geochemistry, Geophysics, Geosystems*, *7*(7). https://doi.org/10.1029/2005gc001238

Wessel, P., Luis, J. F., Uieda, L., Scharroo, R., Wobbe, F., Smith, W. H. F., & Tian, D. (2019). The generic mapping tools version 6 [Software]. Zenodo, *20*(11), 5556–5564. (Funded by US National Science Foundation grants OCE-1558403 and EAR-1829371). https://doi.org/10.5281/zenodo.3407866

White-Gaynor, A. L., Nyblade, A. A., Aster, R. C., Wiens, D. A., Bromirski, P. D., Gerstoft, P., et al. (2019). Heterogeneous upper mantle structure beneath the Ross Sea Embayment and Marie Byrd Land, West Antarctica, revealed by P-wave tomography. *Earth and Planetary Science Letters*, *513*, 40–50. https://doi.org/10.1016/j.epsl.2019.02.013

Wiens, D. A., Aster, R., & Bromirski, P. (2014). Collaborative Research: Collaborative Research: Dynamic response of the ross ice shelf to ocean waves and structure and dynamics of the ross sea from a passive seismic deployment on the ross ice shelf [Dataset]. International Federation of Digital Seismograph Networks. https://doi.org/10.7914/SN/XH_2014

Wiens, D. A., & Nyblade, A. (2007). A broadband seismic experiment to image the lithosphere beneath the Gamburtsev Mountains, East Antarctica [Dataset]. International Federation of Digital Seismograph Networks. https://doi.org/10.7914/SN/ZM_2007

Wiens, D. A., Nyblade, A., & Aster, R. (2007). IPY POLENET-Antarctica: Investigating links between geodynamics and ice sheets [Dataset]. International Federation of Digital Seismograph Networks. https://doi.org/10.7914/SN/YT_2007

Wiens, D. A., Shen, W., & Lloyd, A. (2021). The seismic structure of the Antarctic upper mantle. In *Memoirs*. Geological Society. M56-2020–18. https://doi.org/10.1144/m56-2020-18

Wilson, D. S., & Luyendyk, B. P. (2009). West Antarctic paleotopography estimated at the Eocene-Oligocene climate transition. *Geophysical Research Letters*, *36*(16). https://doi.org/10.1029/2009gl039297

Winberry, P. J., & Anandakrishnan, S. (2003). Seismicity and neotectonics of West Antarctica. *Geophysical Research Letters*, *30*(18). https://doi.org/10.1029/2003GL018001

Xie, J., Ritzwoller, M. H., Brownlee, S., & Hacker, B. (2015). Inferring the oriented elastic tensor from surface wave observations: Preliminary application across the western United States. *Geophysical Journal International*, *201*(2), 996–1021. https://doi.org/10.1093/gji/ggv054

Xie, J., Ritzwoller, M. H., Shen, W., Yang, Y., Zheng, Y., & Zhou, L. (2013). Crustal radial anisotropy across Eastern Tibet and the Western Yangtze Craton. *Journal of Geophysical Research: Solid Earth*, *118*(8), 4226–4252. https://doi.org/10.1002/jgrb.50296

Yao, H., van der Hilst, R. D., & Montagner, J. (2010). Heterogeneity and anisotropy of the lithosphere of SE Tibet from surface wave array tomography. *Journal of Geophysical Research: Solid Earth*, *115*(B12). https://doi.org/10.1029/2009jb007142

Zhou, Z., Wiens, D. A., Shen, W., Aster, R. C., Nyblade, A., & Wilson, T. J. (2022). Radial anisotropy and sediment thickness of West and Central Antarctica estimated from Rayleigh and Love wave velocities. *Journal of Geophysical Research: Solid Earth*, *127*(3). https://doi.org/10.1029/2021jb022857

Zhu, H., Bozdağ, E., & Tromp, J. (2015). Seismic structure of the European upper mantle based on adjoint tomography. *Geophysical Journal International*, *201*(1), 18–52. https://doi.org/10.1093/gji/ggu492

Zhu, H., Komatitsch, D., & Tromp, J. (2017). Radial anisotropy of the North American upper mantle based on adjoint tomography with US Array. *Geophysical Journal International*, *211*(1), 349–377. https://doi.org/10.1093/gji/ggx305

Zhu, H., Yang, J., & Li, X. (2020). Azimuthal anisotropy of the north American upper mantle based on full waveform inversion. *Journal of Geophysical Research: Solid Earth*, *125*(2). https://doi.org/10.1029/2019jb018432